CFD STUDY ON THE EFFECT OF TUBES DIAMETER AND COUNT ON FLOW DISTRIBUTION UNIFORMITY IN A Z DISPOSITION

by

Mohamed A. KARALI[a*], Mathkar A. ALHARTHI[b], Bandar Awadh ALMOHAMMADI[c], Mohamed H. MOHAMED[d], Hassanein A. REFAEY[b,e], Mostafa A. H. ABDELMOHIMEN[e,f], and Hytham A. Abd EL-GHANY[g,h]

[a] Department of Mechanical Engineering, Faculty of Engineering and Technology, Future University in Egypt, New Cairo, Egypt
[b] Department of Chemical Engineering, College of Engineering at Yanbu, Taibah University, Yanbu Al-Bahr, Saudi Arabia
[c] Department of Mechanical Engineering, College of Engineering at Yanbu, Taibah University, Yanbu Al-Bahr, Saudi Arabia
[d] Mechanical Engineering Department, College of Engineering and Islamic Architecture, Umm Al-Qura University, Makkah, Saudi Arabia
[e] Department of Mechanical Engineering, Faculty of Engineering at Shoubra, Benha University, Cairo, Egypt
[f] Department of Mechanical Engineering, King Khalid University, Abha, Saudi Arabia
[g] Department of Engineering Mathematics and Physics, Faculty of Engineering at Shoubra, Benha University, Cairo, Egypt
[h] Department of Physics, College of Science, Taibah University, Al-Madinah Al-Munawarah, Saudi Arabia

Original scientific paper
https://doi.org/10.2298/TSCI220922049K

The present paper goal is to compile a comprehensive database of data on the pressure drop and flow distribution uniformity utilizing CFD in a network of parallel tubes arranged in a Z configuration adopted for flat plate solar collectors. A 3-D CFD model is implemented to simulate such a system as in the market, including two domains: tube materials and fluid, besides entering, and exiting prolonged ports. The model specifications are Z disposition of uniform inlet and outlet headers diameter (D = 20 mm), length of 1150 mm, and tube length of 1780 mm. The investigated design parameters include the number of tubes (N = 5, 10, and 15) and the tubes diameter to header diameter ratio (d/D = 0.25, 0.35, and 0.50). For a wide range of inlet Reynolds numbers from 500-5000. The present model demonstrated noticeable agreement with offered experimental findings from the literature. The results affirmed that lowering both the number of tubes and the diameter of tubes enhances the flow distribution uniformity. The findings indicate that lowering the number of tubes from 15 to 5 at a lower tubes diameter to header diameter ratio of of 0.25 at a higher Reynolds number yields a maximum increase in flow distribution uniformity of roughly 180% with a negative effect on the total pressure drop.

Key words: *flow distribution, pipes networks, CFD, Z disposition, flat plate solar collector*

* Corresponding author, e-mails: mkarali@fue.edu.eg, mohamedkarali@yahoo.com

Introduction

Solar energy takes a lot of importance in the last years and the researchers used the solar energy in several important applications which can change the lifestyle in world by reducing the usage of the fossil oil [1-12]. Parallel piping connections of *Z* disposition are popularly used within flat plate solar collectors. It consists of an inlet distributing header, a companying outlet header, and an array of parallel tubes between the two headers. In reality, and due to some assembly considerations, the tubes array is extended into the dividing and combining headers for a few millimeters producing the entering and prolonged exit ports. The moving fluid-flows from the entering header to the outlet header passing through the array of tubes. In *Z* disposition, fluid passes through the inlet header and is consequently gathered and left from the network in the same direction. Generally, in parallel piping connections, flow distribution uniformity (FDU) beside pressure drops both affect the performance (Weitbrecht *et al.* [13], and Duffie and Beckman [14]). For such a system, the FDU and reducing pressure drop will minimize the pumping power and improve the system's efficiency. Developments according to the newest manufacturing techniques, measuring devices, and software. But, due to difficulties in performing experimental works with such systems or even hard to implement, the CFD simulations represent an appropriate alternative solution.

Weitbrecht *et al.* [13] performed experiments on isothermal flow dividing in *Z*-shaped flat plate solar collectors using laser doppler velocimetry techniques. Moreover, they forecast the fluid-flow concentration dispersal for different cases using mathematical models. Tubes' prolonged ports (junctions) of 4.5 mm were considered for both inlet and exit headers. The results concluded a dependence of the fluid-flow concentration distribution on the Reynolds number, as larger Reynolds numbers generate larger gradients in the flow distribution. Bassiouny and Martin [15, 16] presented a mathematical model based on mass and momentum conservation equations in plate heat exchangers with parallel channels for two dispositions of *Z* and *U*. They studied the system pressure drop and relative FDU. The results stated a principle for the total pressure that it is equal for the two configurations, *U* and *Z*. Jones and Lior [17] numerically examined the flow distribution across a particular solar arrangement of *Z* and *U* structures for 54 distinct patterns. Ahn *et al.* [18] presented two parameters that can be used in analyzing the FDU in distributing manifolds at low Reynolds number: the ratio of manifold diameter and manifold length at inlet and outlet. They produced a correlation for the optimum FDU as a function of the Reynolds number and the two ratios.

Maharudrayya *et al.* [19] presented a 1-D mathematical model relays on mass and momentum conservation equations in the entering and exhaust gas headers of *Z* and *U* constructions in planar fuel cells. The results have been validated with those obtained from 3-D CFD simulations applying CFX code. Fan *et al.* [20] performed a CFD study and experimental works on the flow and temperature profile inside solar panels consisting of inclined channels. They reported that in some positions, the moving fluid gets boiling due to maldistribution. Fang *et al.* [21] have built a model adapted to match the natural phenomena physics to predict the pressure variations in headers of heat exchangers. Their model has been experimentally validated. Wang [22] introduced an intensive literature survey on manifold FDU and compared different CFD, discrete and analytical models. A generalized model has been produced for uniform and varied cross-section manifold designs. Ekramian *et al.* [23] showed a numerical methodology to study the influence of many parameters on the thermal performance of flat plate solar collectors. The experimental work of Cruz-Peragon *et al.* [24] was also used to confirm the numerical results of their fluid-flow concentration distribution. Hassan *et al.* [25] used numerical and physical mod-

els to look at how the FDU increases in sections of different manifolds that are the same length or get smaller as they go along. When a tapered manifold with a ratio of two was used instead of a uniform one, the results showed that FDU went up. Facao [26] made a model that uses correlations for pressure loss to find the best way to design a manifold. The optimized model was tested numerically and in the real world. His research showed that for better FDU, the diameter of the combining manifold should be more significant than the diameter of the dividing manifold. Yang *et al.* [27] have used numbers to study what happens when the rectangular exit ports in a distribution manifold have different aspect ratios. The results showed that an aspect ratio of 0.25 was best for practical work.

Karvounis *et al.* [28] have numerically and experimentally researched the FDU in a *Z*-shaped flat plate solar collector. Experiments included measuring each riser's fluid mass-flow rate using the ultrasound technique. Based on their results, it is found that the non-uniformity among risers increases along with the increase of the inlet fluid-flow rate. Further, they used CFD to examine how changing the diameter of each riser tube affected the FDU's performance. A tiny model with 10 channels integrated into two rectangular manifolds was represented numerically, and experimental results for the flow distribution in *U*- and *Z*-type configurations were also provided by Siddiqui *et al.* [29]. The results demonstrated that the U configuration manifold had superior FDU at higher Re. To improve FDU in parallel pipe networks, several methods were implemented to investigate various factors. Modifications are possible to the number of absorber tubes, their diameters, the manifold to tube diameter ratio, the size and shape of the manifold and header, and more. Karali *et al.* [30] recently used CFD to simulate the pipe connection for a *Z*-shaped flat plate solar collector. A 3-D model is built with components, including tubes, fluid domains, and regular entrance and exit ports. These studies examined the impact of different tapered longitudinal sections of manifolds on the homogeneity and consistency of flow allocation. The findings showed that to improve the FDU, a unique taper ratio should be adopted per each inlet Reynolds number.

The findings determined that a different taper ratio should be used for each inlet Reynolds number to maximize the FDU's effectiveness. Considering the previous sections, it could be summarized that very few CFD models can be found to model such systems as in reality. Including the two domains, tube materials and fluid, entering and exiting prolonged ports. This is related to complex geometry and the expensive computational facilities required. However, accomplishing such CFD works would reveal an excellent agreement of the CFD results compared to the experimental observations if available. That introduces such CFD works to substitute needed experimental tests, especially for many studied cases and even difficult designs to implement in laboratories. In this sense, the idea of the present paper was designed to perform an intensive CFD analysis considering the system as it looks in the market with the minimum assumptions needed. Aims to provide an extensive information database about the FDU and pressure drop of a *Z* disposition parallel tubes. Under the influence of changing many design parameters will be discussed in the next section. That would be helpful in the design and optimization processes for such systems. The model dimensions are taken from the experimental work of Weitbrecht *et al.* [13].

Numerical methods

Problem statement

The computational domain is chosen in this research to match the experimental model developed by Weitbrecht *et al.* [13] to validate the proposed CFD model. Where flat plate solar

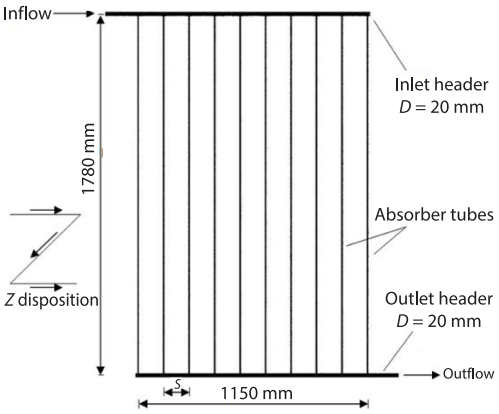

Figure 1. Specifications of *Z* disposition; sample – main case, *N* =10 tubes and *S* = 127 mm

collectors were commercialized and given the proportions used today. A horizontally placed *Z* disposition replicates the water FDU in a 3-D model. The model's parameters are shown in fig. 1 as constant entrance and exit headers with diameters of 20 mm and lengths of 1150 mm for the headers and tubes, respectively (1780 mm). The analyzed design factors are listed in tab. 1 of the CFD program used for this work, allowing the analysis of nine alternative *Z* disposition. A sizable collection of data is made available by the CFD findings to aid in designing and optimizing such systems.

Table 1. The CFD investigated parameters

d/*D*	*N*	$\dot{m}$ [kgs^{-1}]/Re$_D$						
0.25 (*d* = 5 mm)	5	0.0078 500	0.0157 1000	0.0236 1500	0.0314 2000	0.0472 3000	0.0629 4000	0.0787 5000
	10							
	15							
0.35 (*d* = 7 mm)	5							
	10							
	15							
0.50 (*d* = 10 mm)	5							
	10							
	15							

Where d is the tube diameter, D – the headers diameter (D = 20 mm), N – the total tubes number, Re$_D$ – the Reynolds number at the header entering is obtained based on from eq. (1), $\dot{m}$ – the fluid total rate of mass-flow at the inlet, and μ – the fluid dynamics viscosity coefficient [31]:

$$\mathrm{Re}_D = \frac{4\dot{m}}{\pi D\mu} \tag{1}$$

Geometrical parameters

The problem geometry is a 3-D model sketched utilizing ANSYS-Design Modeler R18.0. There are nine different dispositions; all are similar in the main dimensions of the *Z* disposition as illustrated in fig. 1. In contrast, each disposition has detailed specifications of tube diameter (d = 5 mm, 7 mm, and 10 mm) and the number of tubes (N = 5, 10, and 15). The distance between tubes (center to center – S) varies according to the number of tubes. The S is 285.75 mm, 127 mm, and 81.643 mm, for the designs, N = 5, N = 10, and N = 15, respectively, as shown in figs. 2(a)-2(c). Figure 2(d) depicts the prolonged ports. The entering and exit extended ports of the absorber tubes have 4.5 mm inside the two headers, entering and exit (taken exactly from Weitbrecht *et al.* [13]. Therefore, the current CFD model is close to natural systems in the market and is expected to match better results from experimental work. Figures 2(e) and 2(f) illustrate the fluid and tube bodies, respectively.

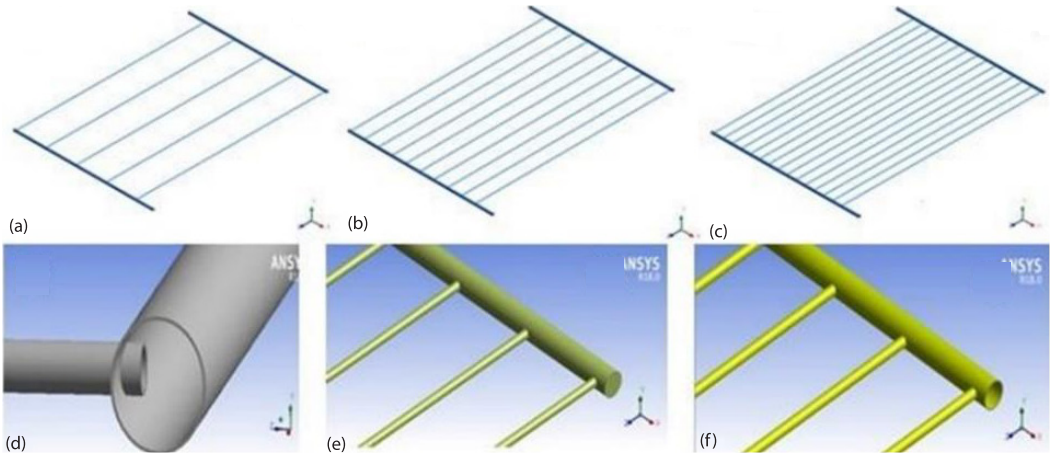

Figure 2. Photos from design modeler; (a) $N = 5$, (b) $N = 10$ tubes, (c) $N = 15$ tubes, (d) prolonged ports of absorber tubes with headers (junctions), (e) fluid body, and (f) tubes and headers body

Mesh specifications and independence study

In such CFD problems, a fine grid is needed because of the large aspect ratio of the length of the tube to the tube's diameter. Moreover, inflation layers can be used to capture the flow behavior inside the boundary-layer. Therefore, a thorough grid analysis is required to optimize the number of cells without compromising numerical convergence and outcomes. Using ANSYS-ICEM Mesh R18.0, a tetrahedron-based 3-D uniform volume mesh is created. The mesh quality for all studied cases was ensured using mesh skewness of 0.9. Figure 3 shows a sample mesh creation for both domains. A mesh independence test is performed using five grids as illustrates in tab. 2. The mean fluid-flow velocity from five dispersed planes throughout the riser length (U for the first and final tubes is computed using the given domains, boundary conditions, the laminar turbulence model, and the convergence criterion. Table 2 tabulates the grid test study for one case. It shows that increasing the cell count above 6266817 yields marginal changes in the fluid velocities values, so it is proposed to use grid 3 to all cases (9 dispositions) in the current work. Intel (R) Xeon (R) CPU X5650 2.67 GHz 24 GB RAM operating in parallel local MPI was the computing capability used.

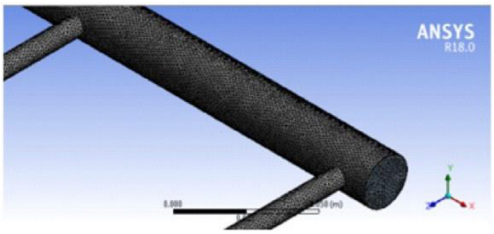

Figure 3. Sample mesh creation (both domains) utilizing ANSYS-ICEM R18.0

Solution set-up

The ANSYS-CFX Solver R18.0 is utilized in this work. The solution set-up is two domains were identified: fluid domain (water) and pipes domain (copper). The fluid domain boundary conditions are fluid inlet mass-flow rate at the inlet that corresponds to Re_D value range from 500 to 5000, including seven points: 500, 1000, 1500, 2000, 3000, 4000, and 5000, pressure outlet (0 bar) at fluid outlet. The tubes domain boundary condition: walls with the no-slip condition at the inner surfaces. The convergence criterion was set to residual mean square with a residual value of 10^{-7}. The conservation equations of mass and momentum for Newtonian incompressible steady flow can be written:

$$\frac{\partial u}{\partial x}+\frac{\partial v}{\partial y}+\frac{\partial w}{\partial z}=0 \tag{2}$$

Momentum conservation equation in x-direction:

$$\rho\left(u\frac{\partial u}{\partial x}+v\frac{\partial u}{\partial y}+w\frac{\partial u}{\partial z}\right)=-\frac{\partial p}{\partial x}+\mu\left(\frac{\partial^2 u}{\partial x^2}+\frac{\partial^2 u}{\partial y^2}+\frac{\partial^2 u}{\partial z^2}\right) \tag{3}$$

Simulations were performed for steady-state and no energy conditions. A simple method was used for the pressure velocity coupling and a high resolution second order for the momentum.

Table 2. Mesh independency study (d = 7 mm, d/D = 0.35, N = 10, and Re_D = 2000)

	Total number of cells	Mean fluid-flow velocity, $\bar{U}$ [ms^{-1}]	
		Tube 1	Tube 10
Grid 1	4105722	0.0775426	0.09783391
Grid 2	5707797	0.0771973	0.0959673
Grid 3	6266817	0.0785025	0.09033489
Grid 4	8345644	0.0786426	0.09335532
Grid 5	16924698	0.0786627	0.09060163

Turbulence model and validation

The current model was validated against available experimental results from Weitbrecht *et al.* [13]. Their experimental results are the measured fluid-flow concentration ($FFC = Q_i/Q_t$) per each absorber tube in a Z disposition of headers diameter (D = 20 mm), tube diameter (d = 7 mm), number of tubes (N = 10), and for four different inlet Re_D = 807, 1491, 2555, and 4604. The flow rate per each absorber tube, Q_i, is calculated based on the average fluid velocity passing through the tube from five planes distributed over the tube length, $\bar{U}_i$, [24]:

$$Q_i=\frac{\pi}{4}d^2\bar{U}_i \tag{4}$$

The fluid-flow concentration (FFC_i) is calculated as a ratio from the total outlet flow rate, Q_t, as presented:

$$FFC_i=\frac{Q_i}{Q_t} \tag{5}$$

However, picking the suitable turbulence model is the first step toward reliable outcomes. For the higher Re_D example (Re_D = 4604), Weitbrecht *et al.* [13] evaluated the three turbulence models listed in tab. 3: the k-ε model, the k-ε SST model, and the laminar model. Based on the results in tab, 3, it is clear that the laminar model is the most appropriate one to be used in all study since it exhibits minor fluctuation (3.6%). In theory, this is feasible as even at the maximum Re_D value (>2000), Re_D (locally) within risers stays in the laminar area. Some other researchers have reached the same conclusion based on what was revealed, Karvounis *et al.* [28]. In tab. 4, we can see how the present CFD model compares to the experimental findings of Weibrecht *et al.* [13].

Table 4 shows that the FFC calculated using the current model is quite close to the experimental values found by Weitbrecht *et al.* [13].

Table 3. Turbulence model test against exp. results of [13] at Re_D = 4604, D = 20 mm, d = 7 mm, and N = 10

Absorber tube, i	Experiomental results	CFD, k-ε model	CFD, k-ω SST model	CFD, laminar model
1	0.0869	0.0869	0.0927	0.0851
2	0.0889	0.0889	0.0932	0.0881
3	0.0896	0.0906	0.0936	0.0903
4	0.0899	0.0934	0.0953	0.0929
5	0.0933	0.0957	0.0972	0.0963
6	0.0986	0.1000	0.0993	0.0990
7	0.1031	0.1040	0.1018	0.1029
8	0.1100	0.1082	0.1050	0.1087
9	0.1171	0.1135	0.1092	0.1152
10	0.1261	0.1189	0.1126	0.1215
Maximum deviation	–	5.7%	10.6%	3.6%

Table 4. Validation of the present model with experimental results from Weitbrecht *et al.* [13] (D = 20 mm, d = 7 mm, and N = 10

Absorber tube, i	Re_D = 807		Re_D = 1491		Re_D = 2552		Re_D = 4604
	Experimental	CFD	Experimental	CFD	Experimental	CFD	Experimental
1	0.0935	0.0965	0.0927	0.0943	0.0910	0.0919	0.0869
2	0.0956	0.0964	0.0932	0.0945	0.0917	0.0926	0.0889
3	0.0963	0.0962	0.0937	0.0946	0.0924	0.0928	0.0896
4	0.0963	0.0967	0.0960	0.0960	0.0943	0.0948	0.0899
5	0.0988	0.0998	0.0962	0.0989	0.0955	0.0973	0.0933
6	0.1006	0.0985	0.0986	0.0990	0.0977	0.0988	0.0986
7	0.1018	0.1004	0.1006	0.1011	0.1010	0.1017	0.1031
8	0.1036	0.1031	0.1044	0.1043	0.1059	0.1058	0.1100
9	0.1071	0.1051	0.1080	0.1072	0.1108	0.1101	0.1171
10	0.1080	0.1072	0.1120	0.1102	0.1157	0.1142	0.1261
Maximum deviation	–	3.2%	–	2.8%	–	1.9%	–

Assessment of the fluid-flow concentration uniformity

In the present study, the quantification of the flow non-uniformity from the uniform one is conducted based on the dimensionless local fluid-flow concentration non-uniformity parameter, θ_i, that expresses the ratio of the fluid-flow concentration per absorber tube, eq. (5), to the constant value, as indicated in eq. (6), N is the number of absorber tubes:

$$\theta_i = \frac{FFC_i}{FFC_{i,uniform}} = \frac{Q_i / Q_t}{1/N} \tag{6}$$

Two dimensionless indices are used to express the non-uniformity of the studied cases. The $\Delta\theta$, is an index for the difference between the maximum and minimum local non-uniformity per absorber tube, as indicated in eq. (7) [28]. The more significant value indicates the higher difference between the maximum and minimum local non-uniformity per absorber tube:

$$\Delta\theta = 100 \times \left(\theta_{\mathrm{i,max}} - \theta_{\mathrm{i,min}}\right) \quad [\%] \tag{7}$$

The ϕ is an index of the non-uniformity, the standard deviation of the local non-uniformity per each absorber tube for each specified case, as indicated by eq. (8) [28]. The more considerable value of ϕ indicates the higher non-uniformity:

$$\phi = 100 \times \sqrt{\frac{1}{n}\sum_{1}^{n}\left(\theta_{\mathrm{i}} - 1\right)^2} \quad [\%] \tag{8}$$

The CFD results

The FFC distribution results

The results of FFC per each absorber tube, Q_i/Q_t, along with inlet Reynolds number for all studied cases are presented in figs. 4-6. The FFC at lower Reynolds number is characterized by little fluctuations around the uniform distribution-line (dashed black line). However, these fluctuations differ from one case to another. Also, it is seen that the far the absorber tube from the header enters, the higher the FFC. This becomes more noticeable as the Re_D increases as the flow is much affected by inertia force rather than a vicious one. The same finding concerning the FFC among absorber tubes for dispositions of the same type has also been reported in the literature [13, 18, 28]. More remarks will be discussed in the non-uniformity indices section. The three cases; $d = 5$ mm ($d/D = 0.25$), $d = 7$ mm ($d/D = 0.35$), and $d = 10$ mm ($d/D = 0.5$) that illustrated in figs. 4-6 demonstrate that, for same number of tubes as the tube to diameter ratio increase the flow ratio increases. At greater Re_D, the largest improvement in flow ratio was 117%, occurring at a tube count of 15. This improvement was due to an increase in

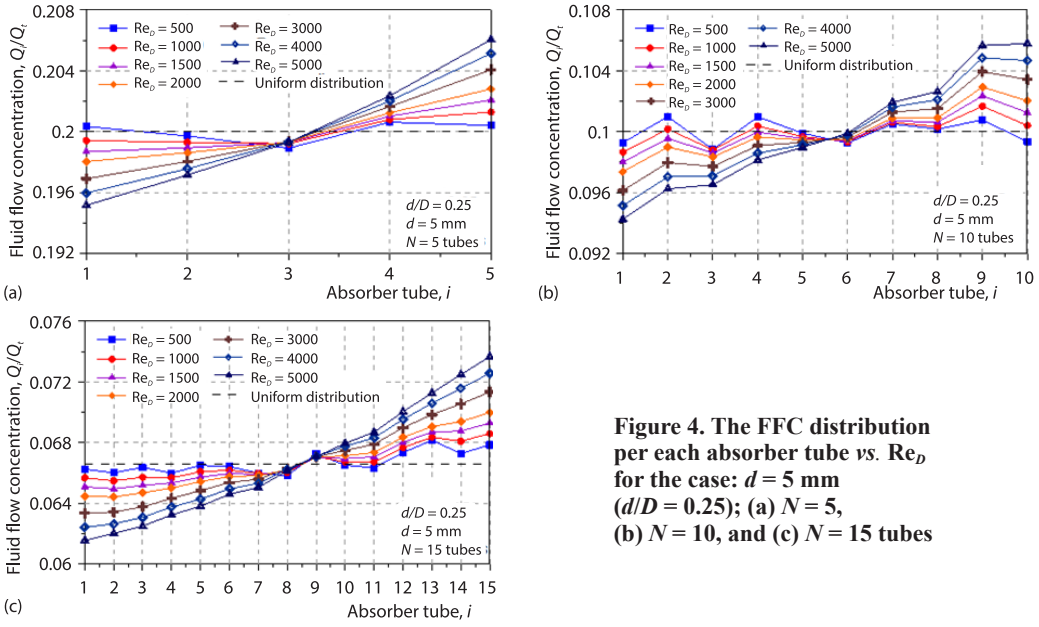

Figure 4. The FFC distribution per each absorber tube *vs.* Re_D for the case: $d = 5$ mm ($d/D = 0.25$); (a) $N = 5$, (b) $N = 10$, and (c) $N = 15$ tubes

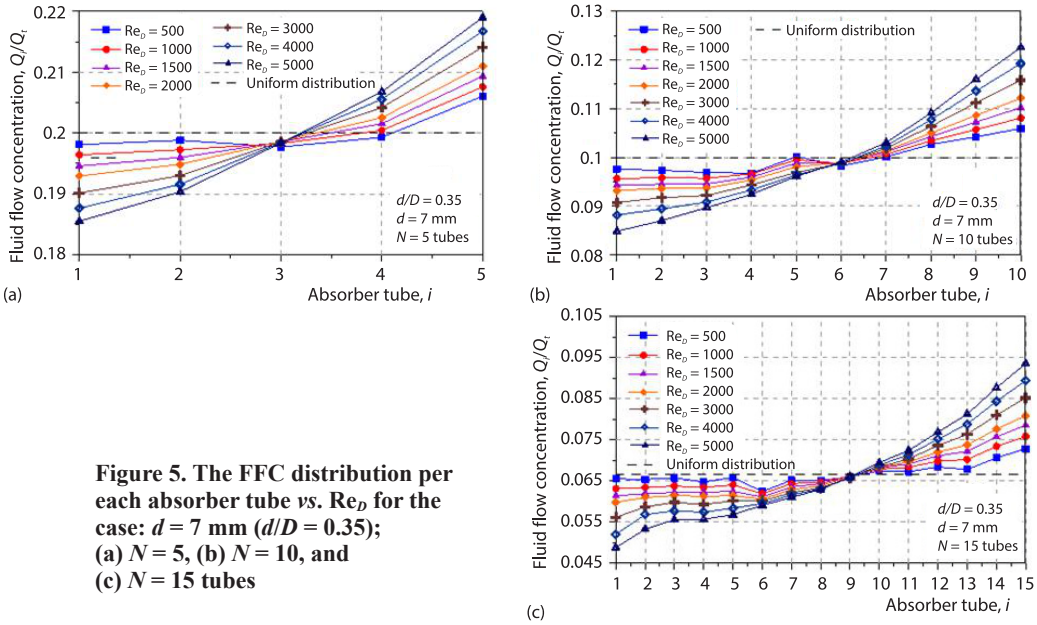

Figure 5. The FFC distribution per each absorber tube *vs.* Re_D for the case: $d = 7$ mm ($d/D = 0.35$); (a) $N = 5$, (b) $N = 10$, and (c) $N = 15$ tubes

the tube-to-diameter ratio from 0.25 to 0.5. By comparison, lowering the tube count from 15 to 5 at a smaller tube to diameter ratio at a larger Re_D results in a maximum increase in flow ratio of roughly 180%. We may explain this by noting that the impact becomes more noticeable at higher Reynolds numbers. Therefore, a bigger Re_D may be to blame for the maldistribution, and the ratio of flow relies on it. As flow is controlled more by inertia than viscosity.

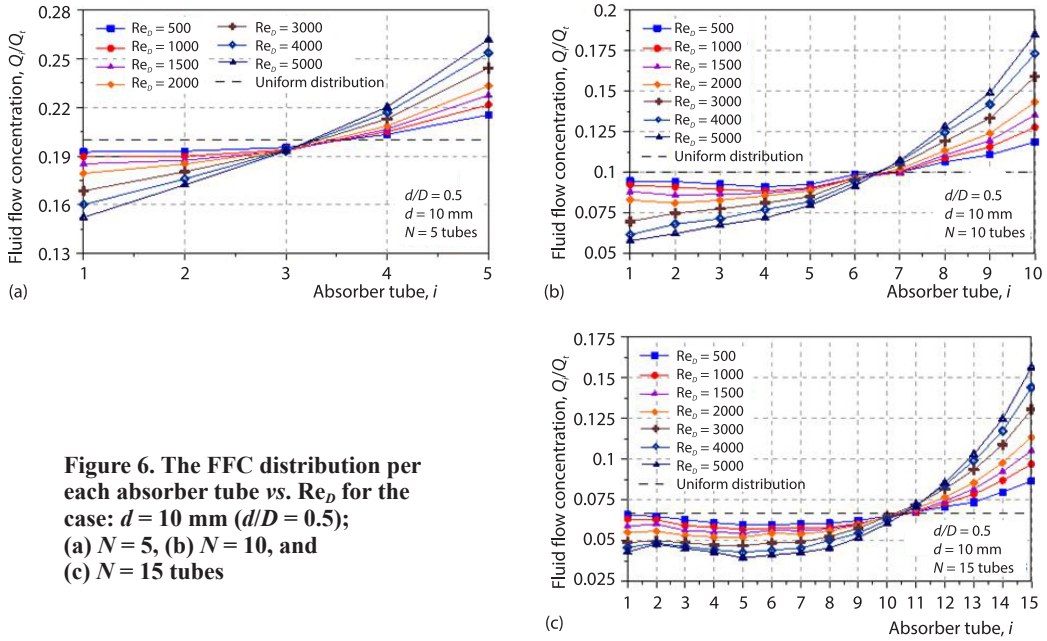

Figure 6. The FFC distribution per each absorber tube *vs.* Re_D for the case: $d = 10$ mm ($d/D = 0.5$); (a) $N = 5$, (b) $N = 10$, and (c) $N = 15$ tubes

Non-uniformity indices

It is essentially required for more clarification of the FFC distribution from the resulting CFD works, an analysis based on the non-uniformity as aforementioned indices, eqs. (9) and (10). Figures 7(a) and 7(b) show the variation of non-uniformity index, $\Delta\theta$, and the non-uniformity index, ϕ, respectively as a function of Re_D. Figure 7(b) affirms the concluding remarks from the previous section of FFC graphs. As it becomes apparent from fig. 7(b), the higher the Re_D, the higher the index of non-uniformity, ϕ.

It could also be deduced from fig. 7(b) that, at a specific tube diameter and Re_D, the increase in the number of tubes leads to higher non-uniformity. As an example, for the case of $d = 7$ mm ($d/D = 0.35$), increasing the number of tubes from 5-15, causes an increase in ϕ from 1.5-3.6 at $Re_D = 500$ and from 5.9-19.2 at $Re_D = 5000$. For the influence of the tube diameter on the index of non-uniformity, ϕ, it could be seen from fig. 7(b) that, at a specific number of tubes and Re_D, the increase in the tube diameter leads to higher non-uniformity, the same conclusion is found in Jones and Lior [17]. For example, for the case of $n = 10$ tubes, increasing the tube diameter from 5-10 mm or d/D from 0.25-0.5 causes an increase in the non-uniformity index from 0.7-8.7 at $Re_D = 500$ and from 3.7-40.0 at $Re_D = 5000$.

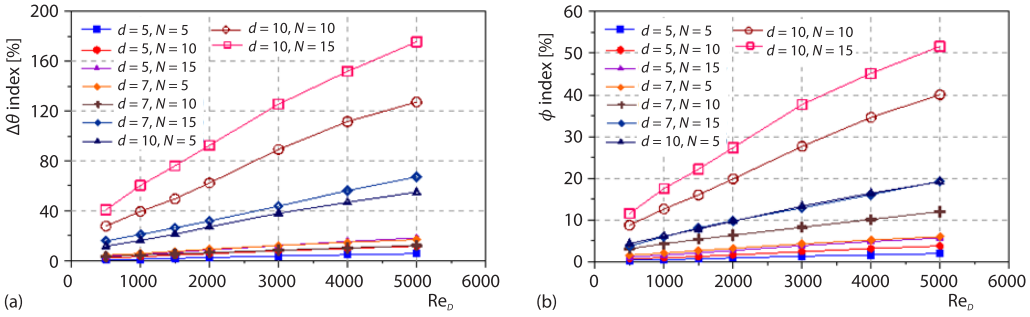

Figure 7. Indices of non-uniformity *vs.* Re_D for all studied cases; (a) $\Delta\theta$ and (b) ϕ

Velocity contours

Few selected velocity contours at only interesting sections and for specified conditions are shown in figs. 8(a)-8(d). Because of the large aspect ratio between the diameter and length of the tube, it is difficult to capture photographs from the resulting velocity contours for the entire system at once. Where, figs. 8(a) and 8(b) are associated to the case of $d = 5$, and $N = 5$, fig. 8(a) $Re_D = 500$, and fig. 8(b) $Re_D = 5000$, while figs. 8(c) and 8(d) are for the case of $d = 10$, and $N = 15$, fig. 8(c) $Re_D = 500$, and fig. 8(d) $Re_D = 5000$. These cases are selected to demonstrate the resulting FFC distribution non-uniformity values described in the last section. Generally, it is found that resulted velocity contours match the FFC distribution non-uniformity values well. As fig. (8) confirmed, the FFC non-uniformity is mainly combined with the higher Re_D values. On the contrary, at lower Re_D, the FDU is enhanced regardless of the other investigated parameters, tube diameter, and the number of tubes.

System total pressure drop

In the present study, the overall pressure drop is obtained as the difference between mean fluid pressure at the entering and exit. Figure 9 graphs the system's total pressure drop results for all studied cases along with Re_D. It is shown in fig. 9 that increasing the inlet Re_D causes a severe increase in the total pressure drop at specific conditions of tube diameter and

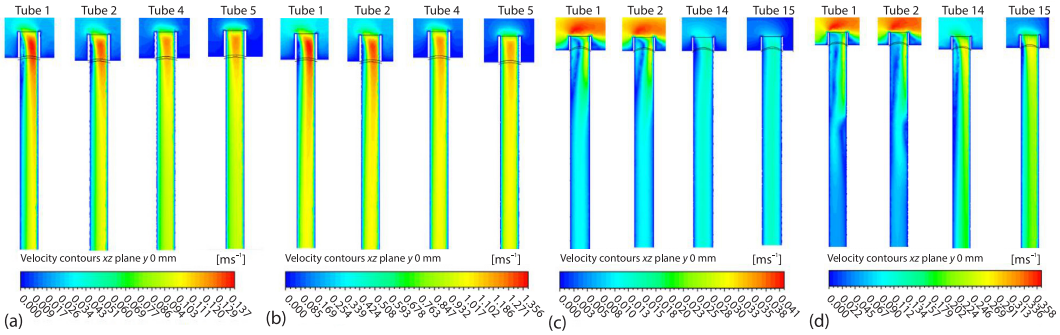

Figure 8. Selected velocity contours; (a) Re_D = 500, d = 5 mm, N = 5, (b) Re_D = 5000, d = 5 mm, N = 5, (c) Re_D = 500, d = 10 mm, N = 15, and (d) Re_D = 5000 d = 10 mm, N = 15

the number of tubes. Indicating higher pumping power needed and poor system efficiency. It could also be observed from fig. (9) that, at a specific tube diameter and Re_D, increasing the number of tubes causes a decrease in the total pressure drop of the system. As an example, for the case of d = 7 mm (d/D = 0.35), increasing the number of tubes from 5-15, causes a decrease in the total pressure drop from 47.7-17.3 at Re_D= 500 and from 663.5-264.5 at Re_D = 5000. The same remark could be observed when studying the influence of increasing the tube diameter at a specific number of tubes and Re_D. For example, for the case of N = 10 tubes, increasing the tube diameter from 5-10 mm, causes a decrease in the total pressure drop from 87.8-8.1 at Re_D = 500 and from 1066.8-179.2 at Re_D= 5000.

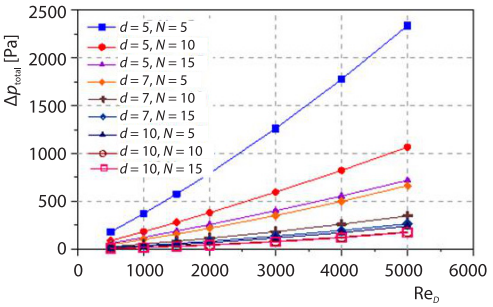

Figure 9. Total pressure drop variation *vs.* Re_D for all studied cases

Conclusions

In this study, a parallel tube network with Z disposition is investigated to build a comprehensive database on the FDU and pressure drop. The CFD analysis is used by various design parameters to depict a flat plate solar collector as it is found in reality. A 3-D CFD model is suggested taking into account two domains of fluid and tubes, as well as the inlet and exit ports. A good agreement was discovered when the current model was validated using experimental findings from the literature. The number of tubes, the ratio of tube diameter to header diameter, non-uniformity indices, and Reynolds number is only a few of the characteristics that have been demonstrated in the current research.

Based on all the available results over the investigated ranges, it could be deduced the following remarks.

- At lower ReD, the distribution of fluid-flow concentration, FFC, is characterized by small variations around the value of uniform distribution.
- The large the far the riser tube from the header enters, the higher the FFC. This becomes more noticeable as the Re_D increases.
- At higher Reynolds number, the largest improvement in flow ratio was 117%, occurring at a tube count of 15 when tube-to- header diameter ratio increases from 0.25-0.5.

- While, lowering the tube count from 15-5 at a smaller tube to diameter ratio at a larger Re_D results in a maximum increase in flow ratio of roughly 180%.
- Hence it is important to note that, optimizing the design parameters is essential while keeping the Re_D at the lowest possible value.
- To reduce the overall pressure loss throughout the system, increase the number of tubes or their diameter. However, the non-uniformity index ϕ shows an opposite trend to this.

Declaration-of-competing-interests

The authors declare that they have no known competing financial interests or personal relationships that could have appeared to influence the work reported in this paper.

Acknowledgment

The Fourth author would like to thank the Deanship of Scientific Research at Umm Al-Qura University for supporting his work by Grant No. 23UQU4361231DSR001.

Nomenclature

d – tube inner diameter, [mm]
D – headers inner diameters, [mm]
$\dot{m}$ – fluid total rate of mass-flow, [kg/s]
N – total tubes number
p – pressure, [Pa]
Q – fluid rate of volume flow, [m^3s^{-1}]
Re_D – Reynolds number
S – distance between tubes, [mm]
U – disposition
U – mean fluid-flow velocity, [ms^{-1}]
Z – Z disposition

Greek symbols

θ_i – local fluid-flow concentration
non-uniformity index, [–]
μ – fluid coefficient of dynamic viscosity, [Pa·s]
ϕ – index of non-uniformity, [%]

Subscripts

i – order of absorber tube, (1, 2, 3....15)
t – total outlet

Acronyms

FDU – flow distribution uniformity
FFC – fluid-flow concentration
max – maximum
min – minimum

References

[1] Prakasam, M. J. S., *et al*., An Experimental Study of the Mass-Flow Rates Effect on Flat-Plate Solar Water Heater Performance Using Al_2O_3/Water Nanofluid, *Thermal Science*, *21* (2017), Suppl. 2, S379-S388
[2] Noghrehabadi, A., *et al*., An Experimental Study of the Thermal Performance of the Square and Rhombic Solar Collectors, *Thermal Science*, *22* (2018), 1B, pp. 487-494
[3] Korres, D. N., Tzivanidis, C., Thermal Analysis of a Serpentine Flat Plate Collector and Investigation of the Flow and Convection Regime, *Thermal Science*, *23* (2019), 1, pp. 47-59
[4] Charoensawan, P., *et al*., Flat Plate Solar Water Heater with Closed-Loop Oscillating Heat Pipes, *Thermal Science*, *25* (2021), 5A, pp. 3607-3614
[5] Hashemian, M., *et al*., Effect of Various Configurations of Swirl Generator System on the Hydrothermal Performance of the Flat-Plate Solar Collector, *Alexandria Engineering Journal*, *66* (2023), 03, pp. 573–595
[6] Rimar, M., *et al*., Analysis and CFD Modelling of Thermal Collectors with a Tracker System, *Energies*, *15* (2022), 6586
[7] Fatahian, H., *et al*., Improving the Flow Uniformity in Compact Parallel-Flow Heat Exchangers Manifold Using Porous Distributors, *Journal of Thermal Analysis and Calorimetry*, *147* (2022), July, pp. 12919-12931
[8] Twaha, S., *et al*., Applying Grid-Connected Photovoltaic System as Alternative Source of Electricity to Supplement Hydro Power Instead of Using Diesel in Uganda, *Energy*, *37* (2012), 1, pp. 185-194
[9] Salah El-Din, M. M., On the Optimization of Solar-Driven Refrigerators, *Renewable Energy*, *20* (2000), 1, pp. 87-93

[10] Abdullah, A. A., *et al*., Measurements of the Performance of the Experimental Salt-Gradient Solar Pond at Makkah one Year after Commissioning, *Solar Energy*, *150* (2017), 1, pp. 212-219
[11] Abdel Dayem, A. M., AlZahrani, A., Psychometric Study and Performance Investigation of an Efficient Evaporative Solar HDH Water Desalination System, *Sustainable Energy Technologies and Assessments*, *52A* (2022), 102030
[12] Hassan, M. K., *et al*., Investigation the Performance of PV Solar Cells in Extremely Hot Environments. *Journal of Umm Al-Qura University for Engineering and Architecture*, *13* (2022), Sept., pp. 18-36
[13] Weitbrecht, V., *et al.*, Flow Distribution in Solar Collectors with Laminar Flow Conditions, *Solar Energy*, *73* (2002), 6, pp. 433-441
[14] Duffie, J. A., Beckman, W. A., Solar Engineering of Thermal Processes, in: *Flat Plate Collectors*, 4th ed., Chapter 6, John Wiley and Sons, Inc, New York, USA, 2013, pp. 236-321
[15] Bassiouny, M. K., Martin, H., Flow Distribution and Pressure Drop in Plate Heat Exchangers – I U Configuration, *Chem. Eng. Sci.*, *39* (1984), 4, pp. 693-700
[16] Bassiouny, M. K., Martin, H., Flow Distribution and Pressure Drop in Plate Heat Exchangers – II Z Configuration, *Chem. Eng. Sci*., *39* (1984b), 4, pp. 701-704
[17] Jones, G. F., Lior, N., Flow Distribution in Manifold Solar Collectors with Negligible Buoyancy Effects, *Solar Energy*, *52* (1994), 3, pp. 289-300
[18] Ahn, H., *et al.*, Flow Distribution in Manifolds for Low Reynolds Number Flow, *KSME International Journal*, *12* (1998), 1, pp. 87-95
[19] Maharudrayya, S., *et al*., Flow Distribution and Pressure Drop in Parallel-Channel Configurations of Planar Fuel Cells, *Journal Power Sources*, *144* (2005), 1, pp. 94-106
[20] Fan, J., *et al*., Flow Distribution in a Solar Collector Panel with Horizontally Inclined Absorber Strips *Solar Energy*, *81* (2007), 12, pp. 1501-1511
[21] Fang, L., *et al*., Analytical and Experimental Investigation of Flow Distribution in Manifolds for Heat Exchangers, *Journal Hydrodyn*, *20* (2008), 2, pp. 179-185
[22] Wang, J., Theory of Flow Distribution in Manifolds, *Chem. Eng. J*., *168* (2011), 3, pp. 1331-1345
[23] Ekramian, E., *et al.*, Numerical Analysis of Heat Transfer Performance of Flat Plate Solar Collectors. Journal of Fluid-Flow, *Heat and Mass Transfer Avestia Publishing*, *1* (2014), Jan., pp. 38-42
[24] Cruz-Peragon, F., *et al*., Characterization of Solar Flat Plate Collectors, *Renewable and Sustainable Energy Reviews*, *16* (2012), 3, pp. 1709-1720
[25] Hassan, J. M., *et al.*, Modelling the Uniformity of Manifold with Various Configurations, *Hindawi Publishing Corporation Journal of Fluids*, *2014* (2014), 10, 325259
[26] Facao, J., Optimization of Flow Distribution in Flat Plate Solar Thermal Collectors with Riser and Header Arrangements, *Solar Energy*, *120* (2015), Oct., pp. 104-112
[27] Yang, H., *et al.*, Effect of the Rectangular Exit-Port Geometry of a Distribution Manifold on the Flow Performance, *Appl. Therm. Eng*., *117* (2017), May, pp. 481-486
[28] Karvounis, P., *et al*., Numerical and Experimental Study of Flow Characteristics in Solar Collector Manifolds, *Energies MDPI*, *12* (2019), 1431
[29] Siddiqui, O. K., *et al*., Flow Distribution in U - and Z -Type Manifolds: Experimental and Numerical Investigation, *Arabian Journal for Science and Engineering*, *45* (2020), June, pp. 6005-6020
[30] Karali, M. A., *et al*., Influence of Using Different Tapered Longitudinal Section Manifolds in a Z Shaped Flat Plate Solar Collector on Flow Distribution Uniformity, *Case Studies in Thermal Engineering*, *33* (2022), 101922
[31] Incropera, F., Dewitt P. D., *Introduction Heat Transfe*r, 6th edition, John Wiley and Sons Inc., New York USA, 2011

Paper submitted: September 22, 2022
Paper revised: January 10, 2023
Paper accepted: February 6, 2023